Published in final edited form as:
J Comp Neurol. 2009 February 1; 512(4): 500–513. doi:10.1002/cne.21909.

"Fast" Plasma Membrane Calcium Pump PMCA2a Concentrates in GABAergic Terminals in the Adult Rat Brain

ALAIN C. BURETTE[1,*], **EMANUEL E. STREHLER**[2], and **RICHARD J. WEINBERG**[1,3]

1*Department of Cell and Developmental Biology, University of North Carolina, Chapel Hill, North Carolina 27599*

2*Department of Biochemistry and Molecular Biology, Mayo Clinic College of Medicine, Rochester, Minnesota 55905*

3*Neuroscience Center, University of North Carolina, Chapel Hill, North Carolina 27599*

Abstract

The plasma membrane Ca^{2+}-ATPases (PMCA) represent the major high-affinity Ca^{2+} extrusion system in the brain. PMCAs comprise four isoforms and over 20 splice variants. Their different functional properties may permit different PMCA splice variants to accommodate different kinds of local [Ca^{2+}] transients, but for a specific PMCA to play a unique role in local Ca^{2+} handling it must be targeted to the appropriate subcellular compartment. We used immunohistochemistry to study the spatial distribution of PMCA2a–one of the two major carboxyl-terminal splice variants of PMCA2–in the adult rat brain, testing whether this isoform, with especially high basal activity, is targeted to specific subcellular compartments. In striking contrast to the widespread distribution of PMCA2 as a whole, we found that PMCA2a is largely restricted to parvalbumin-positive inhibitory presynaptic terminals throughout the brain. The only major exception to this targeting pattern was in the cerebellar cortex, where PMCA2a also concentrates postsynaptically, in the spines of Purkinje cells. We propose that the fast Ca^{2+} activation kinetics and high V_{max} of PMCA2a make this pump especially suited for rapid clearance of presynaptic Ca^{2+} in fast-spiking inhibitory nerve terminals, which face severe transient calcium loads.

Keywords

calcium extrusion; calcium pump; immunohistochemistry; parvalbumin; presynaptic terminals; fast-spiking basket cells

Ca^{2+} signaling plays a central role in neurons. To regulate different functions independently within spatially restricted zones, neurons compartmentalize their Ca^{2+} signals within microdomains. Thus, within a single neuron characteristic ensembles of Ca^{2+} channels, transporters, and binding proteins are found at distinct locations within the soma, axon, and dendrites (Bootman et al., 2001; Rizzuto, 2001). Growing evidence shows that the plasma membrane Ca^{2+}-ATPase (PMCA) family of calcium pumps plays an important role in shaping Ca^{2+} dynamics in these restricted cellular compartments (Strehler et al., 2007a).

An intriguing feature of the PMCA family is its diversity. In mammals, four PMCA isoforms are encoded by separate genes. From these four genes, more than 20 distinct PMCAs are generated through alternative splicing (Strehler and Zacharias, 2001; Di Leva et al., 2008).

*Correspondence to: Alain Burette, Dept. of Cell & Developmental Biology, University of North Carolina, CB #7090, Chapel Hill, NC 27599. E-mail: burette@unc.edu

Alternative splicing affects two major regions of the protein: the first intracellular loop (site A), and the C-terminal tail (site C), which includes sites for phosphorylation by protein kinases A and C. Calmodulin binding to the C-tail regulates the activity of the pump. In its absence, the C-tail acts as an autoinhibitory domain of the pump (Penniston et al., 1988). When calmodulin binds, the C-tail dissociates from the catalytic core, thus activating the pump.

The main splice variants generated at the C-terminal site (termed “a” and “b”) differ in their primary amino acid sequence due to a change in reading frame. Functionally, the most notable consequence of C-terminal splicing is a difference in calmodulin and kinase regulation, leading to different kinetics of calmodulin and Ca^{2+} activation of these pumps (Penniston and Enyedi, 1998).

The large number of functionally different PMCAs raises the possibility that specific PMCA variants are optimized for different kinds of [Ca^{2+}] transients (Domi et al., 2007). Different PMCAs may help shape slow tonic Ca^{2+} in some cells and provide rapid Ca^{2+} clearance in others (Strehler et al., 2007b). Consistent with this idea, PMCA isoforms show developmental-, tissue-, and cell-specific patterns (Kip et al., 2006). PMCA isoforms are differentially expressed among different regions of the adult brain, and among different classes of neurons within a single brain region (Burette et al., 2003). Moreover, neurons can restrict PMCA expression to specific subcellular compartments. For example, we recently demonstrated that in cerebellar Purkinje cells, PMCA2 (the main PMCA isoform in the brain) concentrates in dendritic spines (Burette and Weinberg, 2007). Analogously, individual splice variants might be selectively distributed. Such organization could be functionally important, since different C-terminal splice variants of individual PMCA isoforms vary in their basal activity, kinetics, and regulation by modulatory proteins, but little empirical evidence for splice variant specificity is yet available.

Here, we used immunohistochemistry to investigate the spatial distribution of the “a” variant of PMCA2 (PMCA2a) in the adult rat brain, testing whether this splice variant is targeted to specific neuronal compartments. We found that PMCA2a concentrates in parvalbumin-positive inhibitory terminals throughout the brain. The only major exception to this targeting pattern was in the cerebellar cortex, where PMCA2a concentrates postsynaptically in the spines of Purkinje cells. This exquisitely specific targeting reinforces the idea that the multiplicity of PMCA splice variants may allow neurons to use the right calcium pump at the right place.

MATERIALS AND METHODS

Antibody characterization

For PMCA2 and PMCA2a the rabbit polyclonal antibodies NR2 and CR2a (Filoteo et al., 1997) were used, respectively. NR2 was generated against a 15-residue peptide sequence (TNSDFYSKNQRNESS, residues 5–19) in the amino terminus region of rat PMCA2, and CR2a was generated against a 20-residue peptide sequence (SLSNALSSPTSLPPAAAGGG, residues 1149–1168 of PMCA2x/a) in the carboxy terminus region of rat PMCA2a (Filoteo et al., 1997). The specificity of these antibodies was established by Western blots using microsomes from COS cells overexpressing specific PMCAs, and further confirmed in microsomes from rat brain. In both cases, NR2 recognizes two bands at 127 kDa and 132 kDa, corresponding to PMCA2a and PMCA2b, respectively, while CR2a recognizes only one band at 127 kDa. Moreover, staining was absent in the presence of corresponding peptide immunogen (Filoteo et al., 1997). To further verify antibody specificity, we performed immunocytochemistry on brain sections from deafwaddler-2J allele mutant mice (CByJ.A-Ttc7+?Atp2b2dfw-2J/J, stock 002894, Jackson Laboratory, Bar Harbor, ME), reported to lack PMCA2 mRNA and protein (Street et al., 1998), run in parallel with material from control mice and rats. Staining with both antibodies in the dfw2J mutant mice was extremely weak,

exhibiting a “background” pattern unrelated to that seen for controls (data not shown). NR2 and CR2a were used at 1:200 for DAB immunocytochemistry and 1:40,000 for immunofluorescence using tyramide signal amplification.

For VGLUT1, a guinea pig polyclonal anti-VGLUT1 (Chemicon, Temecula, CA; AB5905, lot 24041061) raised against rat VGLUT1 was used. This antibody was affinity-purified using the immunogenic peptide. By sequencing the immunogen peptide (Chemicon, AG208), we found that this antibody was raised against a C-terminus peptide (GATHSTVQPPRPPPPVRDY, Melone et al., 2005). This antibody recognizes a single band of Mr ≈60,000 on immunoblots of synaptic membrane fractions from rat cerebral cortex. Furthermore, immunogold labeling shows that VGLUT1 immunoreactivity is selectively associated with axon terminals forming asymmetric synapses in cerebral cortex and hippocampus.

For GABA, a rabbit polyclonal anti-GABA (Sigma, St. Louis, MO; A2052, lot 052K4827) developed using GABA-BSA as the immunogen was used. The antibody was affinity-purified using the immunogen. It shows positive binding with GABA, and GABA-KLH in a dot blot assay, and negative binding with bovine serum albumin (BSA) (manufacturer's technical information).

For parvalbumin, a monoclonal anti-parvalbumin antibody (Sigma, PARV-19, P-3088) was used. This antibody derived from a hybridoma produced by fusing mouse myeloma cells with splenocytes from a mouse immunized with purified frog muscle parvalbumin. To control for specify, we performed immunohistochemistry on tissue from parvalbumin-knockout and corresponding control mice (gift from Dr. B. Schwaller; University of Fribourg, Switzerland; see Schwaller et al., 2004). No staining was observed in mice lacking parvalbumin.

Tissue preparation

All procedures related to the care and treatment of animals were in accordance with institutional and NIH guidelines. Twelve male Sprague–Dawley rats (200–350 g, Charles River, Raleigh, NC) were used for this study. After inducing deep anesthesia with sodium pentobarbital (60 mg/kg, i.p.), rats were intracardially perfused with heparinized saline followed by 500 mL of fixative. Rats were fixed with 4% paraformaldehyde freshly depolymerized in phosphate buffer (PB, 0.1 M, pH 7.4) for light microscopy (LM), or with a mixture of 4% paraformaldehyde and 0.1% glutaraldehyde in PB for EM. Brains were then removed and postfixed for 2 hours at 4°C in the same fixative. Brains were cut at 40–60 μm on a Vibratome and collected in cold PB.

Single labeling

Free-floating sections were permeabilized with 50% ethanol for 30 minutes and then treated for 30 minutes with 3% H_2O_2 in phosphate-buffered saline (PBS, 0.1 M, pH 7.4). After pre-incubation in 10% normal donkey serum (NDS, to block secondary antibody binding sites), sections were incubated in primary antibody overnight on a shaker at room temperature. For immunoperoxidase microscopy, sections were then incubated for 3 hours in biotinylated secondary antibody (1:200; Jackson ImmunoResearch, West Grove, PA) and for 1 hour in ExtrAvidin-peroxidase complex (1:5,000; Sigma); peroxidase was histochemically visualized with diaminobenzidine. Processed sections were mounted on gelatin-coated slides, airdried, and cleared with xylene before being coverslipped with D.P.X. mountant (BDH Chemicals, Poole, UK). For immunofluorescence microscopy, immunoreactivity was visualized by donkey IgG, conjugated to Cy-3 (Jackson ImmunoResearch). Sections were then mounted on gelatin-coated slides and directly coverslipped with Vectashield (Vector Laboratories, Burlingame, CA). To control for method specificity, some sections were processed as above,

except that primary or secondary antibodies were omitted. In all such cases, staining was completely absent.

Multiple labeling

Tyramide signal amplification (TSA) was used for multiple labeling with primary antibodies from a single species. Fluorescent staining with the first primary antibody was enhanced with TSA and conventional fluorescent staining was then performed with the second primary antibody. We used the primary antibodies at a concentration so low that antigen consistently failed to be revealed by a conventional fluorophore-conjugated secondary antibody (donkey antirabbit IgG conjugated to FITC; 1:200 for 3 hours, Jackson), but was still clearly detectable with TSA. After overnight incubation in primary antibody, sections were reacted for 2 hours at room temperature with biotinylated secondary antibody (1:200, Jackson). Biotin was revealed by FITC conjugated to tyramide (TSA direct kit, PerkinElmer LifeScience, Boston, MA) according to the manufacturer's recommendation. The second primary antibodies were then applied overnight. Immunoreactivity was visualized by donkey secondary antibody conjugated to Cy-3 (Jackson). For triple labeling, the third primary antibody (raised in a different species than the first two primary antibodies) was applied overnight and visualized by a secondary antibody conjugated to Cy5 (Jackson).

Several control procedures were performed for the multiple labeling with TSA. Omission of primary or secondary antibodies resulted in the lack of specific staining in the corresponding channel. Substitution of preimmune serum for primary antibody led to a very weak Nissl-like pattern of staining. To control for possible crossreaction between the first primary antibody and the second secondary antibody, the second primary antibody was omitted. In such cases, no staining was observed on the channel corresponding to the second secondary antibody. Moreover, we obtained identical results when the order of the first two primary antibodies was reversed.

Sections were examined with a Leitz DMR microscope (Leica, Wetzlar, Germany). Images were acquired with a 12-bit cooled charge-coupled device camera (Retiga EX, QImaging, Canada) coupled to a Macintosh computer or with a Leica SP2 confocal microscope. We used Corel Draw v. 12 (Ontario, Canada) to sharpen images, adjust brightness and contrast, and compose final plates.

Electron microscopy

For preembedding EM immunohistochemistry, sections were permeablized with 50% ethanol for 30 minutes and treated with 1% sodium borohydride for 30 minutes to quench free aldehyde groups. Sections were then further processed as for DAB immunoperoxidase staining for LM. Immunoreacted tissue was rinsed in PB, postfixed 1 hour in 1% osmium tetroxide, rinsed in PB, rinsed in 0.1 M maleate buffer (MB; pH 6), stained en bloc for 1 hour in 1% uranyl acetate in MB, rinsed, then dehydrated in a graded ethanol series followed by propylene oxide, infiltrated with a mixture of Epon and Spurr resins, embedded between two sheets of Aclar plastic supported by glass slides, and polymerized at 60°C for 36–48 hours. Thin sections mounted on copper grids were counter-stained with 5% uranyl acetate and Sato's lead and examined on a Philips Tecnai 12 EM (FEI, Hillsboro, OR).

Image analysis

It is difficult to avoid subjective judgments when studying colocalization of puncta. To permit more objective assessment of our double-stained material, we employed two different algorithms designed for this purpose. To estimate the percentage of spatial colocalization we used an algorithm introduced by Costes et al. (2004). First, an intensity threshold (representing an estimated background) for each channel was automatically determined based on a linear

least-squares fit of the green and red intensities in the image's cytofluorogram. Pearson's correlation coefficient (*r*) for the thresholded images was then calculated (Gonzalez and Wintz, 1987). Costes' approach was implemented in ImageJ (NIH, Bethesda, MD) using the JACoP plug-in (Bolte and Cordelieres, 2006; Rasband, 1997–2005).

To test whether staining pairs were positively correlated, negatively correlated, or random, we performed intensity correlation analysis as described by Li et al. (2004). In contrast to standard spatial colocalization tests, which are in essence binary tests of whether two stains occur in the same regions, Li et al.'s method focuses on staining intensity, addressing whether the intensity of staining for the two proteins varies in synchrony. The method involves generating scatterplots of stain A or stain B against the product of the difference of each pixel A and B intensity from its respective means, $(A_i - \bar{A})\ (B_i - \bar{B})$. The intensity correlation analysis results are then presented as a pair of graphs, where the x-axis reflects the covariance of the channel and the y axis reflects the intensity distribution of the channel. Since the analysis is carried out separately for each stain, strong dependence of stain A on B in combination with minimal dependence of B on A can be identified. Distributions that skew to the right indicate positively correlated staining patterns (where the two pixel staining intensity values vary in synchrony); ones that are symmetrical about the 0 axis indicate independent staining; and those that skew to the left indicate negatively correlated staining patterns, where the pixel staining intensity values vary inversely. Intensity correlation analyses were accomplished with the “Intensity Correlation Analysis” plug-in in ImageJ (see the ImageJ Web site established by the Wright Cell Imaging Facility, Toronto Western Research Institute, Ontario, Canada: www.uhnresearch.ca/wcif).

RESULTS

PMCA2a was detected throughout the brain. Staining was strongest in the cerebellar cortex, followed by the superior colliculus and the cerebral cortex (Fig. 1A). Little PMCA2a staining was found in the white matter.

In the spinal cord, PMCA2a staining was detected throughout the gray matter (Fig. 1B). PMCA2a was present in all layers of the dorsal horn, although sparse in lamina II (Fig. 1C). At high magnification, staining appeared punctate; thin processes were also lightly stained, but immunoreactive cell bodies were not seen (Fig. 1D). In the ventral horn, numerous puncta were seen in the neuropil (Fig. 1E). Unstained cell bodies–the largest likely to represent α-motoneurons–were enveloped by PMCA2a-immunoreactive puncta, but were themselves immunonegative (Fig. 1F).

In the cerebellar cortex, PMCA2a concentrated in the molecular layer, with strongest staining in spines (Figs. 2A,B). Small spiny secondary dendrites were also immunopositive, but large aspiny primary dendrites were only weakly stained. A thin layer of PMCA2a staining also covered the somata of Purkinje cells. In the granule cell layer, synaptic glomeruli were stained, but little or no staining was detected in the granule cells themselves. In the cerebellar nuclei, large intensely stained puncta were visible in neuropil; staining surrounded immunonegative neuronal somata (Fig. 2C). Staining was also prominent in vestibular nuclei.

In the superior colliculus, staining was strongest in the superficial gray and other gray layers, where PMCA2a was organized into vertically oriented bands (Fig. 2D,E). In deep layers, staining often surrounded unstained somata (Fig. 2F,G). PMCA2a was present throughout the thalamus (Fig. 3A). Staining concentrated in dense puncta surrounding somata while more weakly stained fibers were observed in the neuropil (Fig. 3B,C). In the neostriatum, PMCA2a staining was confined between fascicles, which themselves exhibited little staining (Fig. 3D). At high magnification, staining was organized into puncta linked by thin processes (Fig. 3E).

In hippocampus, PMCA2a staining concentrated in the pyramidal cell layer of Ammon's Horn (Fig. 4A), where numerous positive puncta covered somata of pyramidal neurons (Fig. 4B,C). Immunopositive puncta were also observed in stratum radiatum and stratum oriens, but at a much lower density; scattered thin processes were also visible (Fig. 4B,C). In the dentate gyrus, staining concentrated in stratum granulosum, where positive puncta covered the somata of numerous granule cells (Fig. 4D). Scattered positive puncta were visible in the hilus and the stratum moleculare.

In the cerebral cortex, staining was found in the neuropil throughout all layers (Fig. 5A). Numerous puncta surrounded unstained somata of pyramidal neurons, especially in layers II/III and V (Fig. 5B). In contrast to our previous work using a pan-PMCA2 antibody, PMCA2a staining appeared quite restricted (compare Fig. 5A,B with 5C,D). To confirm this impression, we performed double-labeling for PMCA2a and pan-PMCA2. PMCA2a staining overlapped with PMCA2 staining throughout the brain (confirming the specificity of the PMCA2a antibody), but PMCA2a represented only a modest fraction of PMCA2 staining. In cerebral cortex, colocalization was prominent around the somata of numerous neurons (Fig. 5E). At high magnification, pyramidal cell somata were covered by a thin layer of PMCA2-positive/PMCA2a-negative staining, likely representing PMCA2b at the somatic plasma membrane (inset in Fig. 5E). These pyramidal neurons were surrounded by a peri-somatic net of puncta double-stained for PMCA2 and PMCA2a.

To reveal the nature of these puncta we performed electron microscopy. PMCA2a immunoreactivity concentrated in axon terminals making symmetric synapses onto axon initial segments or somata (Fig. 5F). Reaction product could be diffuse, but it was usually located in the back of the terminal, away from the synapse. In contrast, axon terminals making symmetric synapses onto dendrites were generally devoid of staining. Moreover, PMCA2a immunoreactivity was not observed in axon terminals making asymmetric synapses onto dendritic spines. Occasionally, we also observed small clumps of PMCA2a reactivity within cell bodies, associated with the endoplasmic reticulum. We concluded that PMCA2a concentrated in a subpopulation of inhibitory axon terminals, but not in excitatory terminals.

Results from LM double-labeling experiments for PMCA2a with VGLUT1 (a marker for excitatory presynaptic terminals) and GABA (a marker for inhibitory presynaptic terminals) further support this conclusion. Visual inspection revealed little evidence for colocalization of PMCA2a with VGLUT1, as documented for cerebral cortex in Figure 6A. Neuronal somata were immunonegative for PMCA2a, but numerous puncta were double-labeled for PMCA2a and GABA; these could be seen surrounding both GABA-positive and GABA-negative somata (Fig. 6B). However, not all perisomatic GABAergic puncta were PMCA2a-positive (Fig. 6C). Taken together, these findings suggest that PMCA2a in cerebral cortex concentrated in a subset of GABAergic presynaptic terminals, but not in glutamatergic terminals.

At least three groups of GABAergic cells in cerebral cortex contribute to somatic innervation: parvalbumin fast-spiking cells; cholecystokinin regular-spiking or burst-spiking nonpyramidal cells; and small VIP regular-spiking or burst-spiking nonpyramidal cells (Kawaguchi and Kubota, 1998). We performed double-labeling experiments, finding that PMCA2a was expressed in a large fraction of parvalbumin-positive terminals (Fig. 7); likewise, the majority of PMCA2a puncta were also immunopositive for parvalbumin. In contrast, dendrites and somata positive for parvalbumin were mostly negative for PMCA2a. Thus, we conclude that in cerebral cortex PMCA2a is expressed selectively in axon terminals of fast-spiking interneurons. PMCA2a was also closely associated with parvalbumin in other parts of the brain. In many regions of the brain, including hippocampus (Fig. 7B), PMCA2a staining was mostly restricted to parvalbumin-positive axon terminals. The only obvious exception to this rule was

in the molecular layer of the cerebellar cortex, where PMCA2a was expressed in the (parvalbumin-positive) spines of Purkinje cells (Fig. 7C,D).

Since visual inspection is inherently subjective and may lead to misinterpretation, we performed quantitative image analysis. We used the method of Costes et al. (2004) to estimate the percentage of colocalization of PMCA2a with other synaptic markers, finding that 92% of PMCA2a staining in cerebral cortex overlapped with PMCA2, whereas only 3.5% of PMCA2 overlapped with PMCA2a, confirming our visual impression that PMCA2a-stained profiles represented a small fraction of all PMCA2-positive structures. For this reason, the Pearson's correlation coefficient for the two channels, although highly significant, was relatively weak ($r = 0.35$). Consistent with our impression that PMCA2a was associated with inhibitory terminals, 83% of PMCA2a staining overlapped with GABA staining, which represented 36% of the total GABA staining ($r = 0.41$); in contrast, PMCA2a and VGLUT showed only ≈2% overlap. Finally, we confirmed the strong relationship between PMCA2a and parvalbumin, finding that 95% of PMCA2a staining overlapped with parvalbumin staining, which represented 22% of the total parvalbumin staining ($r = 0.55 \pm 0.14$).

To gain further insight into the pattern of colocalization, raw confocal images were analyzed using intensity correlation analysis as described by Li et al. (2004). In every region examined, images from material double-labeled for PMCA2a and PMCA2, GABA, or parvalbumin exhibited intensity correlation plots skewed toward the upper right quadrant (Fig. 8), implying that pixels strongly stained for PMCA2a tended also to be positive for the other antigen, consistent with colocalization. In contrast, images from material double-labeled for PMCA2a and VGLUT exhibited intensity correlation plots skewed toward the upper left quadrant (Fig. 8D), implying that pixels strongly stained for PMCA2a tended to be negative for VGLUT. In conclusion, quantitative image analysis confirms that PMCA2a labeling is largely restricted to parvalbumin-positive inhibitory nerve terminals.

DISCUSSION

Here we show that PMCA2a, a major PMCA2 splice variant, is expressed in parvalbumin-positive axon terminals. This selective expression supports the view that PMCAs play an active role in shaping Ca^{2+} dynamics in restricted cellular compartments (Krizaj and Copenhagen, 1998; Morgans et al., 1998; Yamoah et al., 1998; Usachev et al., 2002; Bautista and Lewis, 2004; Scheuss et al., 2006).

The overall pattern of immunostaining for PMCA2a reported here is generally consistent with that shown in a recent report (Jensen et al., 2007). However, our data are at variance with their conclusion that PMCA2a in hippocampus is enriched in excitatory terminals, and regulates excitatory synaptic transmission. While the basis of this discrepancy is unclear, it may in part reflect “noisy” immunostaining or ineffective use of image analysis tools. The confirmatory functional evidence presented in the study by Jensen et al. (2007) relies on a nonspecific ATPase inhibitor (carboxyeosin) that modulates all PMCAs, and possibly also SERCA and Na^+ pumps (Helmich-de Jong et al., 1986; Skou and Esmann, 1981). In the light of the present results, we conclude that the reported enhancement of paired-pulse facilitation observed with carboxyeosin likely reflects an influence on some other PMCA isoform, or perhaps a secondary effect of the drug.

PMCA targeting

Our laboratory previously showed that neurons can organize PMCA isoforms differentially into spatially restricted domains (Burette et al., 2003; Burette and Weinberg, 2007). The present work extends these results, demonstrating that a single splice variant is targeted to a single type of presynaptic terminal. Recent experimental studies in model systems have shown that

alternative splicing can play a major role in PMCA targeting. In epithelial cells the A-splice-site insert regulates PMCA2 targeting to the apical membrane (Chicka and Strehler, 2003). Those authors showed that the size of the insertion at the A-splice site controls PMCA2 apical targeting, regardless of the C-terminal cassette; a 45-amino-acid insert at this site (the w-form) resulted in apical targeting, whereas smaller inserts resulted in basolateral targeting. Other PMCAs may use different targeting mechanisms. For example, the binding of PMCA4b to SAP97 (via its PDZ binding domain) may help to retain the Ca^{2+} pump at the basolateral membrane in epithelial cells (DeMarco and Strehler, 2001).

Functional implication of PMCA2a in parvalbumin terminals

The axon terminal represents a restricted calcium microdomain where small fluxes can lead to massive changes in local $[Ca^{2+}]_i$ (Lisman et al., 2007). The spatiotemporal characteristics of this local signal are shaped by the interplay between Ca^{2+} sources and sinks; control of these Ca^{2+} swings is crucial for the release of neurotransmitter, and for activity-dependent changes in efficacy of transmitter release (Zucker and Regehr, 2002). PMCA has been found in several types of presynaptic terminals including terminals of chick Edinger–Westphal neurons (Fujii et al., 1996), calyx-type presynaptic nerve terminals of the chick ciliary ganglion (Juhaszova et al., 2000), and parallel fiber terminals in cerebellar cortex (Burette and Weinberg, 2007).

The suspicion that PMCAs may play a major role in controlling Ca^{2+} in the terminal has been demonstrated directly in several experimental models, including the motor terminal in *Drosophila* (Lnenicka et al., 2006), the ribbon synapses of vertebrate photoreceptors (Morgans et al., 1998; Johnson et al., 2007), and the calyx of Held (Kim et al., 2005).

Synapses can differ markedly in their efficacy and dynamics, in part due to differences in Ca^{2+} handling. A variety of functional differences have been documented in the release machinery used by excitatory versus inhibitory terminals, but even within the population of GABAergic terminals, abundant evidence points to functional heterogeneity (Freund and Buzsaki, 1996; McBain and Fisahn, 2001; Somogyi and Klausberger, 2005): In both neocortex and hippocampus, parvalbumin marks a distinct class of interneurons, the fast-spiking (FS) basket cells, characterized by high-frequency, nonadapting spike train (Freund and Buzsaki, 1996). Available evidence suggests that FS basket cells may use a specialized Ca^{2+} toolkit. Thus, parvalbumin in FS cells helps to curtail Ca^{2+} transients in their terminals, preventing asynchronous release and adaptation (Aponte et al., 2008). In contrast, the lack of calcium-binding proteins in non-FS basket cells may result in prolonged calcium transients at their synapses after several closely spaced action potentials. Beyond their distinctive content of calcium buffers, it was recently shown that GABA release from FS basket cells is mediated exclusively by P/Q-type VDCCs, whereas GABA release from CCK-positive basket cells is mediated exclusively by N-type VDCC (Hefft and Jonas, 2005). G-protein mediated inhibition of P/Q type VDCCs is weaker than that of the N-type, and voltage-dependent relief of G-protein-mediated inhibition is stronger for P/Q-type channels than for N-type channels. Thus, P/Q-type channels appear especially well suited for repetitive firing at a high and constant rate.

The present data demonstrate that FS terminals express uniquely high levels of PMCA2a. PMCA2a has enzymatic and regulatory properties that may contribute to functional optimization of these axon terminals. Splice variants of PMCA2 have significantly lower K_d values for Ca^{2+} that other PMCAs, and therefore can extrude Ca^{2+} to substantially lower levels than other PMCA isoforms (Elwess et al., 1997). Ensuring low $[Ca^{2+}]_i$ at rest is particularly important in axon terminals: at least one of the Ca^{2+} binding sites involved in activating the transmitter release machinery has a K_d of 10 μM; thus, in order for the release sites to recover fully after activity, local $[Ca^{2+}]$ must be brought to very low resting levels. Likewise, PMCA2 exhibits especially high V_{max}, allowing these terminals to recover quickly after bursts of activity. Moreover, because of its high affinity for CaM, PMCA2 has a slow inactivation rate,

implying that during ongoing activity, PMCA2 will remain "pre-activated," able to respond immediately to the next Ca^{2+} spike (Hilfiker et al., 1994; Elwess et al., 1997; Caride et al., 2001). Finally, PMCA2a (unlike other PMCA2 variants) exhibits exceptionally rapid activation in response to a rise in $[Ca^{2+}]_i$ (Caride et al., 2001). All these characteristics make PMCA2a ideally matched to the Ca^{2+} handling requirements of parvalbumin terminals, permitting reliable transmitter release even during sustained high-frequency firing.

The only notable exception to the general pattern of PMCA2a targeting was in the cerebellar cortex, where PMCA2a was also expressed in the parvalbumin-rich spines of Purkinje cells. However, like parvalbumin terminal, these spines exhibit exceptionally large Ca^{2+} transients, reinforcing the idea that PMCA2a is adapted to function in microdomains requiring rapid control of especially large Ca^{2+} transients.

CONCLUSION

The versatility of Ca^{2+} as an intracellular messenger depends on its spatial and temporal properties. To create Ca^{2+}-signaling systems with different spatial and temporal properties, different cells express different components from a large Ca^{2+}-signaling toolkit. The repertoire of this toolkit is further expanded through alternative splicing. The highly selective expression of PMCA2a in the terminals of fast-spiking interneurons illustrates this principle, demonstrating that functionally different axon terminals use different components from that toolkit to create Ca^{2+} signaling systems with different spatiotemporal properties.

ACKNOWLEDGMENTS

A.B. examined and analyzed the microscopic material, prepared plates, and wrote the article. E.E.S. supplied PMCA2a antibody and helped with article writing. R.J.W. helped with article writing and data analysis. The authors thank S. Grand and K. Phend for histological support.

Grant sponsor: National Institutes of Health (NIH); Grant numbers: NS44306 and NS35527 (to R.J.W.), NS51769 (to E.E.S.).

LITERATURE CITED

Aponte Y, Bischofberger J, Jonas P. Efficient Ca^{2+} buffering in fast-spiking basket cells of rat hippocampus. J Physiol 2008;586:2061–2075. [PubMed: 18276734]

Bautista DM, Lewis RS. Modulation of plasma membrane calcium-ATPase activity by local calcium microdomains near CRAC channels in human T cells. J Physiol 2004;556:805–817. [PubMed: 14966303]

Bolte S, Cordelieres FP. A guided tour into subcellular colocalization analysis in light microscopy. J Microsc 2006;224:213–232. [PubMed: 17210054]

Bootman MD, Lipp P, Berridge MJ. The organisation and functions of local Ca^{2+} signals. J Cell Sci 2001;114:2213–2222. [PubMed: 11493661]

Burette A, Weinberg RJ. Perisynaptic organization of plasma membrane calcium pumps in cerebellar cortex. J Comp Neurol 2007;500:1127–1135. [PubMed: 17183553]

Burette A, Rockwood JM, Strehler EE, Weinberg RJ. Isoformspecific distribution of the plasma membrane Ca^{2+} ATPase in the rat brain. J Comp Neurol 2003;467:464–476. [PubMed: 14624481]

Caride AJ, Filoteo AG, Penheiter AR, Paszty K, Enyedi A, Penniston JT. Delayed activation of the plasma membrane calcium pump by a sudden increase in Ca^{2+}: fast pumps reside in fast cells. Cell Calcium 2001;30:49–57. [PubMed: 11396987]

Chicka MC, Strehler EE. Alternative splicing of the first intracellular loop of plasma membrane Ca^{2+}-ATPase isoform 2 alters its membrane targeting. J Biol Chem 2003;20:18464–18470. [PubMed: 12624087]

Costes SV, Daelemans D, Cho EH, Dobbin Z, Pavlakis G, Lockett S. Automatic and quantitative measurement of protein-protein colocalization in live cells. Biophys J 2004;86:3993–4003. [PubMed: 15189895]

DeMarco SJ, Strehler EE. Plasma membrane Ca^{2+}-atpase isoforms 2b and 4b interact promiscuously and selectively with members of the membrane-associated guanylate kinase family of PDZ (PSD95/Dlg/ZO-1) domain-containing proteins. J Biol Chem 2001;276:21594–21600. [PubMed: 11274188]

Di Leva F, Domi T, Fedrizzi L, Lim D, Carafoli E. The plasma membrane Ca^{2+} ATPase of animal cells: structure, function and regulation. Arch Biochem Biophys 2008;476:65–74. [PubMed: 18328800]

Domi T, Di Leva F, Fedrizzi L, Rimessi A, Brini M. Functional specificity of PMCA isoforms? Ann N Y Acad Sci 2007;1099:237–246. [PubMed: 17446464]

Elwess NL, Filoteo AG, Enyedi A, Penniston JT. Plasma membrane Ca^{2+} pump isoforms 2a and 2b are unusually responsive to calmodulin and Ca^{2+} J Biol Chem 1997;272:17981–17986. [PubMed: 9218424]

Filoteo AG, Elwess NL, Enyedi A, Caride A, Aung HH, Penniston JT. Plasma membrane Ca^{2+} pump in rat brain. Patterns of alternative splices seen by isoform-specific antibodies. J Biol Chem 1997;272:23741–23747. [PubMed: 9295318]

Freund TF, Buzsaki G. Interneurons of the hippocampus. Hippocampus 1996;6:347–470. [PubMed: 8915675]

Fujii JT, Su FT, Woodbury DJ, Kurpakus M, Hu XJ, Pourcho R. Plasma membrane calcium ATPase in synaptic terminals of chick Edinger-Westphal neurons. Brain Res 1996;734:193–202. [PubMed: 8896825]

Gonzalez, RC.; Wintz, P. Digital image processing. Vol. 2nd ed.. Addison-Wesley; Reading, MA: 1987.

Hefft S, Jonas P. Asynchronous GABA release generates long-lasting inhibition at a hippocampal interneuron-principal neuron synapse. Nat Neurosci 2005;8:1319–1328. [PubMed: 16158066]

Helmich-de Jong ML, van Duynhoven JP, Schuurmans Stekhoven FM, De Pont JJ. Eosin, a fluorescent marker for the high-affinity ATP site of (K^+/H^+)-ATPase. Biochim Biophys Acta 1986;858:254–262. [PubMed: 2424502]

Hilfiker H, Guerini D, Carafoli E. Cloning and expression of isoform 2 of the human plasma membrane Ca^{2+} ATPase. Functional properties of the enzyme and its splicing products. J Biol Chem 1994;269:26178–26183. [PubMed: 7929331]

Jensen TP, Filoteo AG, Knopfel T, Empson RM. Presynaptic plasma membrane Ca^{2+} ATPase isoform 2a regulates excitatory synaptic transmission in rat hippocampal CA3. J Physiol 2007;579:85–99. [PubMed: 17170045]

Johnson JE Jr, Perkins GA, Giddabasappa A, Chaney S, Xiao W, White AD, Brown JM, Waggoner J, Ellisman MH, Fox DA. Spatiotemporal regulation of ATP and Ca^{2+} dynamics in vertebrate rod and cone ribbon synapses. Mol Vis 2007;13:887–919. [PubMed: 17653034]

Juhaszova M, Church P, Blaustein MP, Stanley EF. Location of calcium transporters at presynaptic terminals. Eur J Neurosci 2000;12:839–846. [PubMed: 10762313]

Kawaguchi Y, Kubota Y. Neurochemical features and synaptic connections of large physiologically-identified GABAergic cells in the rat frontal cortex. Neuroscience 1998;85:677–701. [PubMed: 9639265]

Kim MH, Korogod N, Schneggenburger R, Ho WK, Lee SH. Interplay between Na^+/Ca^{2+} exchangers and mitochondria in Ca^{2+} clearance at the calyx of Held. J Neurosci 2005;25:6057–6065. [PubMed: 15987935]

Kip SN, Gray NW, Burette A, Canbay A, Weinberg RJ, Strehler EE. Changes in the expression of plasma membrane calcium extrusion systems during the maturation of hippocampal neurons. Hippocampus 2006;16:20–34. [PubMed: 16200642]

Krizaj D, Copenhagen DR. Compartmentalization of calcium extrusion mechanisms in the outer and inner segments of photoreceptors. Neuron 1998;21:249–256. [PubMed: 9697868]

Li Q, Lau A, Morris TJ, Guo L, Fordyce CB, Stanley EF. A syntaxin 1, galpha(o), and N-type calcium channel complex at a presynaptic nerve terminal: analysis by quantitative immunocolocalization. J Neurosci 2004;24:4070–4081. [PubMed: 15102922]

Lisman JE, Raghavachari S, Tsien RW. The sequence of events that underlie quantal transmission at central glutamatergic synapses. Nat Rev Neurosci 2007;8:597–609. [PubMed: 17637801]

Lnenicka GA, Grizzaffi J, Lee B, Rumpal N. Ca^{2+} dynamics along identified synaptic terminals in drosophila larvae. J Neurosci 2006;26:12283–12293. [PubMed: 17122054]

McBain CJ, Fisahn A. Interneurons unbound. Nat Rev Neurosci 2001;2:11–23. [PubMed: 11253355]

Melone M, Burette A, Weinberg RJ. Light microscopic identification and immunocytochemical characterization of glutamatergic synapses in brain sections. J Comp Neurol 2005;492:495–509. [PubMed: 16228991]

Morgans CW, El Far O, Berntson A, Wassle H, Taylor WR. Calcium extrusion from mammalian photoreceptor terminals. J Neurosci 1998;18:2467–2474. [PubMed: 9502807]

Penniston JT, Enyedi A. Modulation of the plasma membrane Ca^{2+} pump. J Membr Biol 1998;165:101–109. [PubMed: 9744998]

Penniston JT, Filoteo AG, McDonough CS, Carafoli E. Purification, reconstitution, and regulation of plasma membrane Ca^{2+}-pumps. Methods Enzymol 1988;157:340–351. [PubMed: 2976465]

Rasband, WS. ImageJ. U. S. National Institutes of Health; Bethesda, MD: 19972008. http://rsb.info.nih.gov/ij/

Rizzuto R. Intracellular Ca^{2+} pools in neuronal signalling. Curr Opin Neurobiol 2001;11:306–311. [PubMed: 11399428]

Scheuss V, Yasuda R, Sobczyk A, Svoboda K. Nonlinear $[Ca^{2+}]$ signaling in dendrites and spines caused by activity-dependent depression of Ca^{2+} extrusion. J Neurosci 2006;26:8183–8194. [PubMed: 16885232]

Schwaller B, Tetko IV, Tandon P, Silveira DC, Vreugdenhil M, Henzi T, Potier MC, Celio MR, Villa AE. Parvalbumin deficiency affects network properties resulting in increased susceptibility to epileptic seizures. Mol Cell Neurosci 2004;25:650–663. [PubMed: 15080894]

Skou JC, Esmann M. Eosin, a fluorescent probe of ATP binding to the (Na^{+}/K^{+})-ATPase. Biochim Biophys Acta 1981;647:232–240. [PubMed: 6170332]

Somogyi P, Klausberger T. Defined types of cortical interneurone structure space and spike timing in the hippocampus. J Physiol 2005;562:9–26. [PubMed: 15539390]

Street VA, McKee-Johnson JW, Fonseca RC, Tempel BL, Noben-Trauth K. Mutations in a plasma membrane Ca^{2+}-ATPase gene cause deafness in deafwaddler mice. Nat Genet 1998;19:390–394. [PubMed: 9697703]

Strehler EE, Zacharias DA. Role of alternative splicing in generating isoform diversity among plasma membrane calcium pumps. Physiol Rev 2001;81:21–50. [PubMed: 11152753]

Strehler EE, Caride AJ, Filoteo AG, Xiong Y, Penniston JT, Enyedi A. Plasma membrane Ca^{2+} ATPases as dynamic regulators of cellular calcium handling. Ann N Y Acad Sci 2007a;1099:226–236. [PubMed: 17446463]

Strehler EE, Filoteo AG, Penniston JT, Caride AJ. Plasma-membrane Ca^{2+} pumps: Structural diversity as the basis for functional versatility. Biochem Soc Trans 2007b;35:919–922. [PubMed: 17956246]

Usachev YM, DeMarco SJ, Campbell C, Strehler EE, Thayer SA. Bradykinin and ATP accelerate Ca^{2+} efflux from rat sensory neurons via protein kinase C and the plasma membrane Ca^{2+} pump isoform 4. Neuron 2002;33:113–122. [PubMed: 11779484]

Yamoah EN, Lumpkin EA, Dumont RA, Smith PJ, Hudspeth AJ, Gillespie PG. Plasma membrane Ca^{2+}-ATPase extrudes Ca^{2+} from hair cell stereocilia. J Neurosci 1998;18:610–624. [PubMed: 9425003]

Zucker RS, Regehr WG. Short-term synaptic plasticity. Annu Rev Physiol 2002;64:355–405. [PubMed: 11826273]

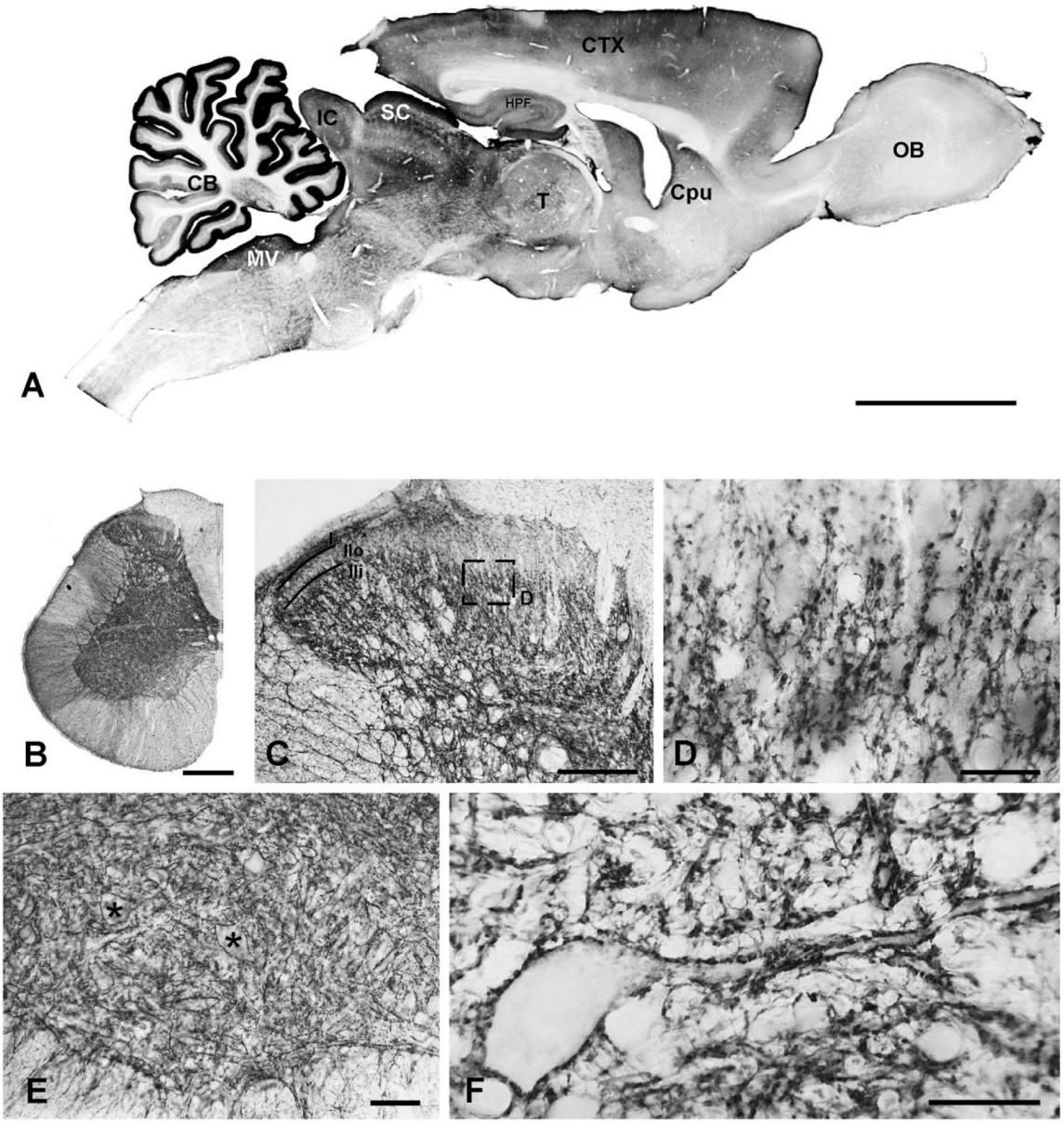

Figure 1.

Distribution of PMCA2a in the brain and the spinal cord. Low-magnification view of immunoperoxidase material shows that PMCA2a is widespread throughout the brain (**A**). Strongest immunostaining is in cerebellar cortex; superior colliculus and cerebral cortex also stain strongly. In the spinal cord, PMCA2a is detected throughout the gray matter (**B**). In the dorsal horn, PMCA2a is detected in all layers, although immunoreactivity is weak in lamina II (**C**). Staining is organized into puncta in the neuropil with thin processes weakly stained (**D**). In the ventral horn, numerous PMCA2a-positive puncta are visible, many of which surround large unstained somata (**F**, stars in **E**). CB, cerebellum; CTX, cerebral cortex; CPu, caudate-putamen; HPF, hippocampal formation; IC, inferior colliculus; MV, medial vestibular nucleus; OB, olfactory bulb T, thalamus; SC, superior colliculus. Scale bars = 0.5 cm in A; 250 μm in B; 100 μm in C; 25 μm in D,F; 50 μm in E.

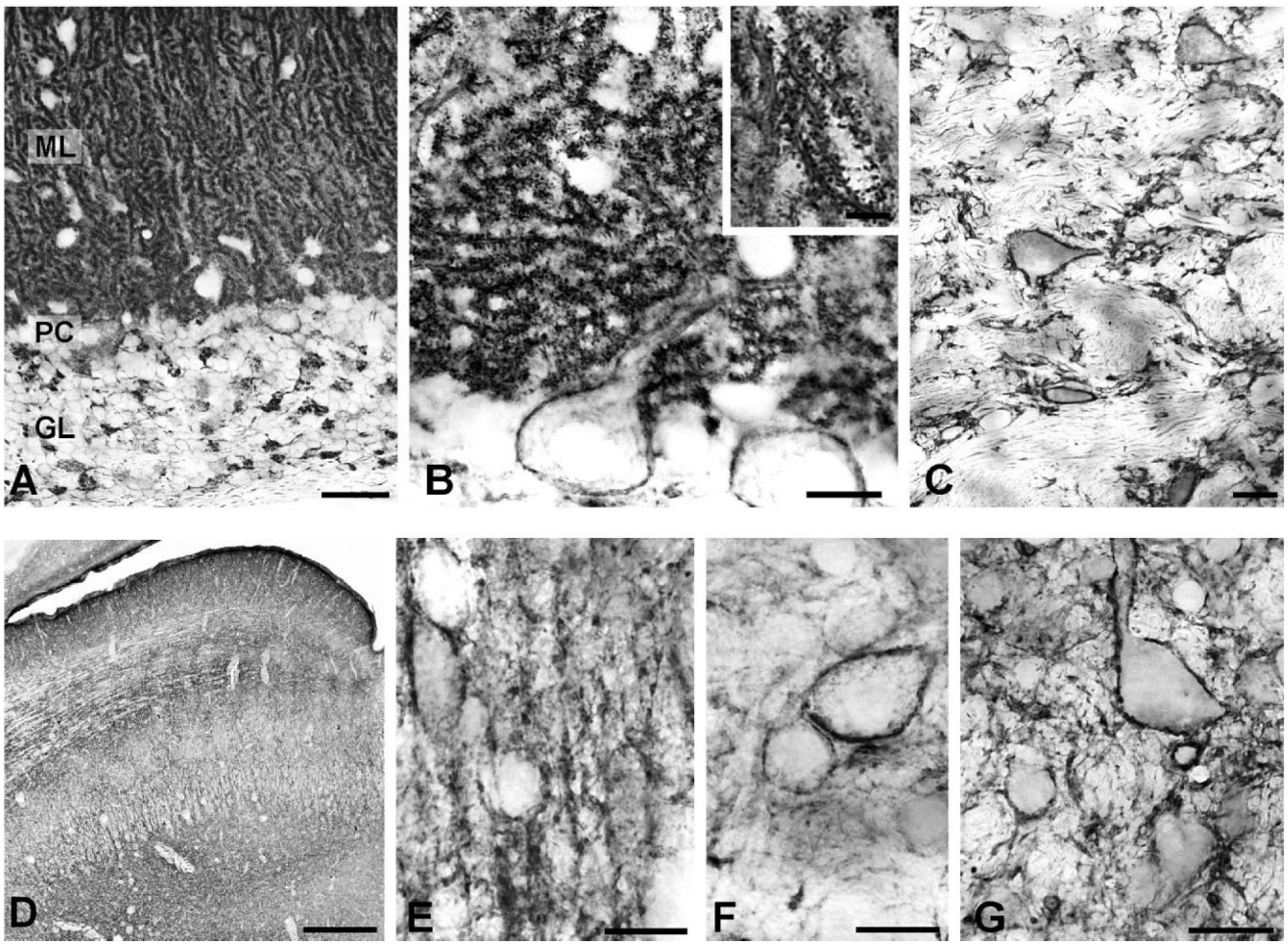

Figure 2.

Distribution of PMCA2a in cerebellum and superior colliculus. PMCA2a is present in all layers of the cerebellar cortex (**A**), strongest in the molecular layer. Higher-magnification view reveals that PMCA2a concentrates in spiny dendrites of Purkinje cells, with a thin layer of staining covering their somata (**B**). Spines in small distal dendrites were strongly immunopositive (inset in B). In deep cerebellar nuclei, PMCA2a staining is patchy, and often surrounds unstained cell bodies (**C**). PMCA2a is detected in all layers of the superior colliculus (**D**). In the superficial gray layer, PMCA2a concentrates in vertically oriented bundles (**E**); in deeper layers it surrounds unstained cell bodies (**F,G**). Scale bars = 50 μm in A; 20 μm in B,E–G; 5 μm in inset in B; 25 μm in C; 0.5 mm in D.

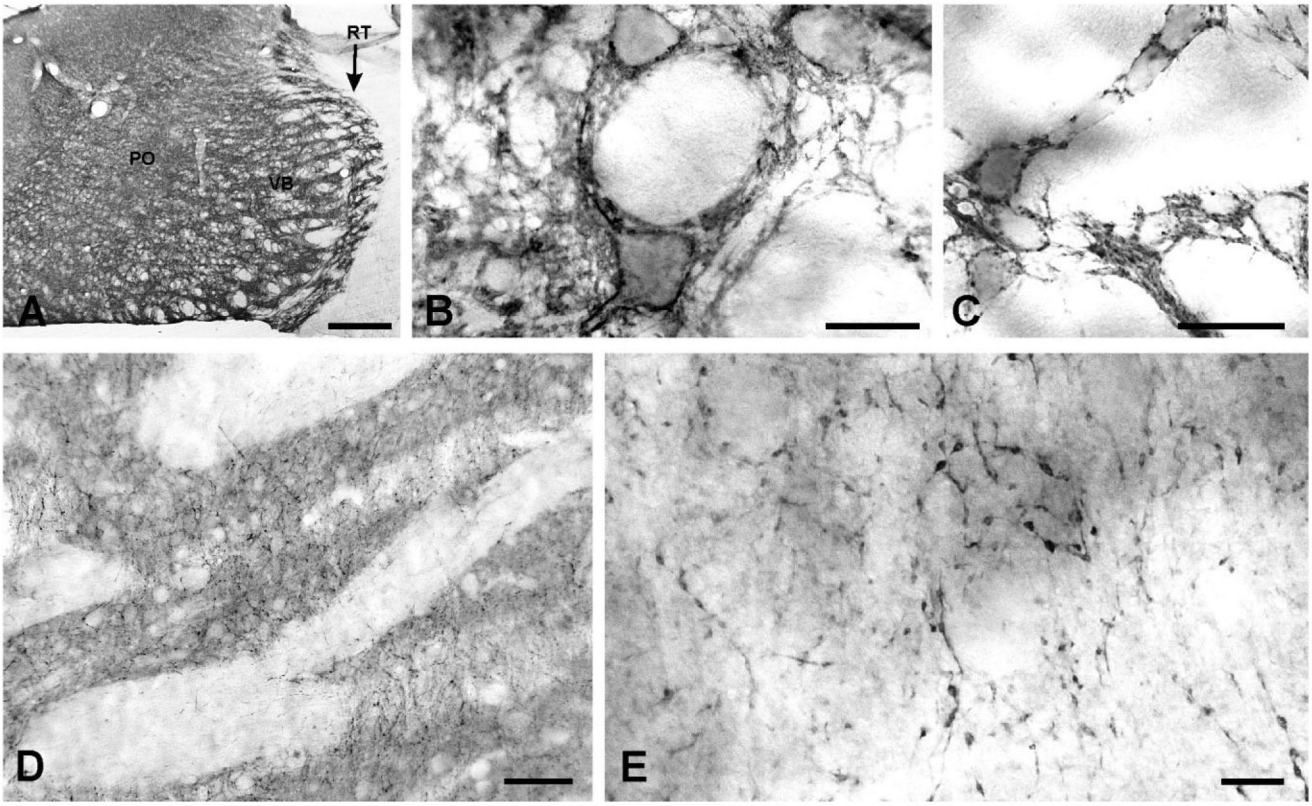

Figure 3.

Distribution of PMCA2a in the thalamus and neostriatum. PMCA2a is present throughout the thalamus (**A**), especially prominent in the parvalbumin-rich reticular nucleus (arrow). Strong staining outlines somata while weakly stained fibers are in the neuropil (**B,C**). In the neostriatum, PMCA2a concentrates in gray matter (**D**); staining is organized into puncta linked by thin processes (**E**). PO, posterior nuclear complex; VB, ventrobasal nuclear complex; RT: reticular thalamic nucleus Scale bars = 500 μm in A; 25 μm in B,C; 100 μm in D; 10 μm in E.

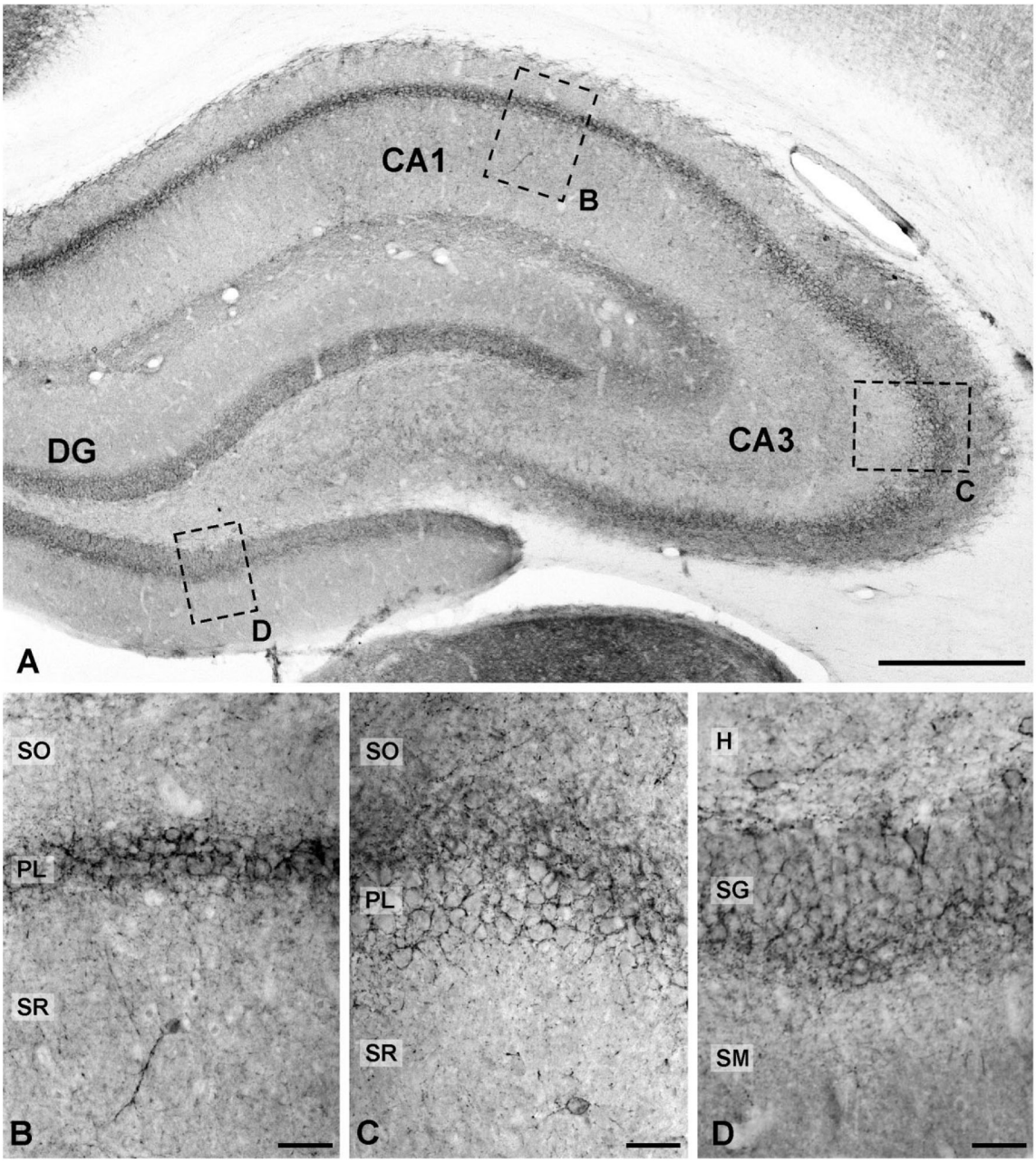

Figure 4.

Distribution of PMCA2a in hippocampus. Overview of PMCA2a staining hippocampus formation (**A**). In CA1 (**B**) and CA3 (**C**) staining is strongest in the pyramidal cell layer (PL), where numerous PMCA2a puncta surround unstained somata. PMCA2a puncta and thin fibers are scattered throughout stratum oriens (SO) and radiatum (SR). In the dentate gyrus, staining is strongest in stratum granulosum (SG) where positive puncta covered the somata of numerous granule cells (**D**). Scattered positive puncta are visible in the hilus (H) and the stratum moleculare (SM). Scale bars = 0.5 mm in A; 50 μm in B–D.

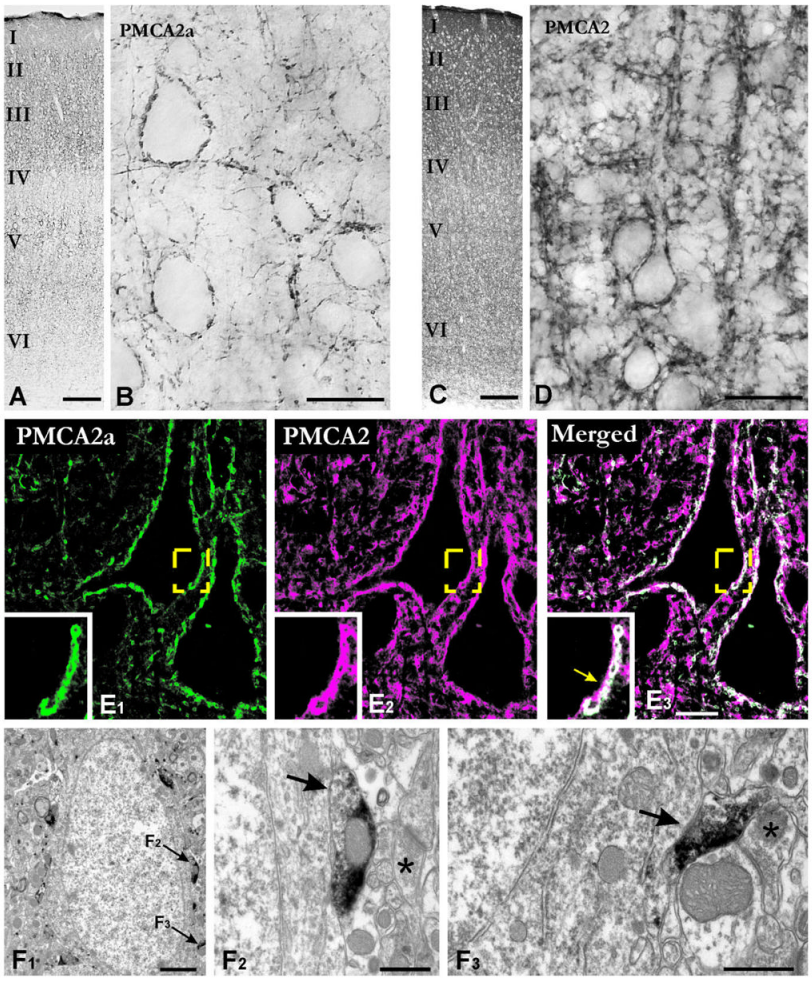

Figure 5.

Distribution of PMCA2 and PMCA2a in the cerebral cortex. Both PMCA2 and PMCA2a stain all layers of the cerebral cortex (**A,C**) but while PMCA2 is relatively uniformly distributed (C), PMCA2a is strongest in layers II/III followed by layer V, and weak in layer I (A). Higher magnification of layer IV shows that PMCA2 is widespread in the neuropil and covers somatic and dendritic plasma membranes (**D**). In contrast, PMCA2a is organized into puncta surrounding unstained somata (**B**); thin fibers are also weakly positive. Double labeling confirms that virtually all PMCA2a staining colocalizes with PMCA2 staining (**E**), whereas a large fraction of PMCA2 staining is unrelated to PMCA2a, likely reflecting the PMCA2b splice variant. High magnification shows that the staining around somata of pyramidal neurons is composed of a thin layer of PMCA2-positive/PMCA2a-negative staining, covered by puncta positive for both PMCA2 and PMCA2a (arrow, inset in E); these PMCA2a puncta often appear hollow. Electron microscopy reveals PMCA2a immunoreactivity in axon terminals making symmetric synapse onto somata (arrows in **F**$_{1–3}$). Within these axon terminals, reaction product was often confined to the back of the terminal, away from the synapse. In contrast, axon terminals making asymmetric synapses onto dendritic spines (asterisk in F_2) or symmetric synapses onto dendrites (asterisk in F_3) are immunonegative. Scale bars = 200 μm in A,C; 25 μm in B,D; 10 μm in E; 2 μm in F_1, 0.5 μm in F_2, 0.5 μm in F_3.

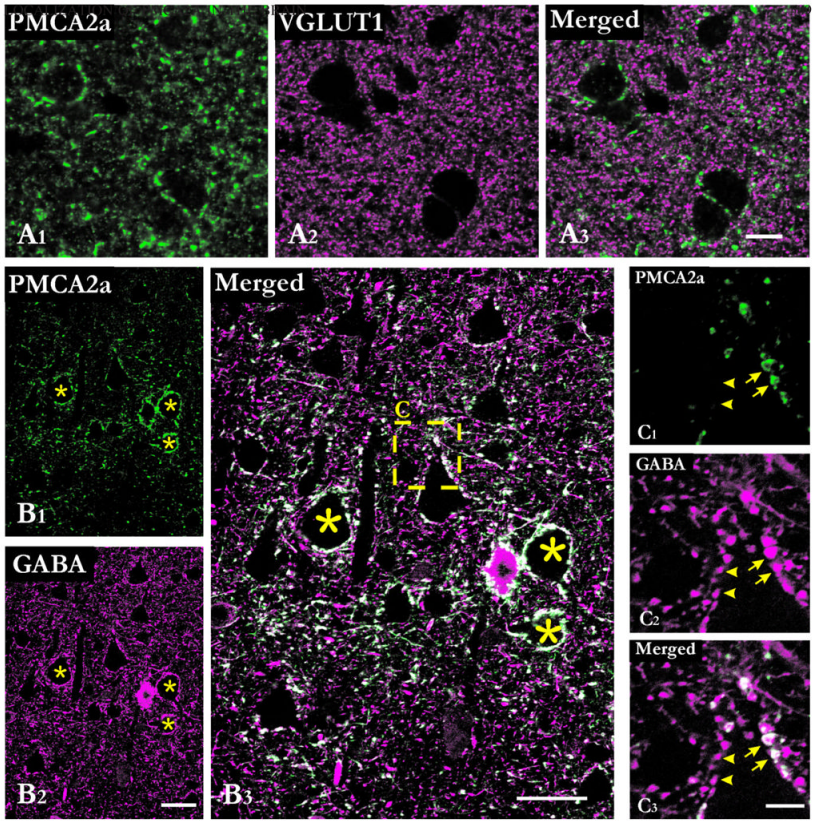

Figure 6.

PMCA2a colocalizes with GABA in a subset of inhibitory nerve terminals. Double immunofluorescence shows little colocalization of PMCA2a with VGLUT (**A**) but extensive colocalization with GABA (**B**). Colocalization is prominent around somata (asterisks). At higher magnification, PMCA2a is present in numerous GABA-positive puncta surrounding somata, but not all GABA-positive puncta are positive for PMCA2a (**C**). This staining pattern suggests that PMCA2a is expressed in a subpopulation of GABAergic axon terminals. Scale bars = 10 μm in A; 25 μm in B; 5 μm in C.

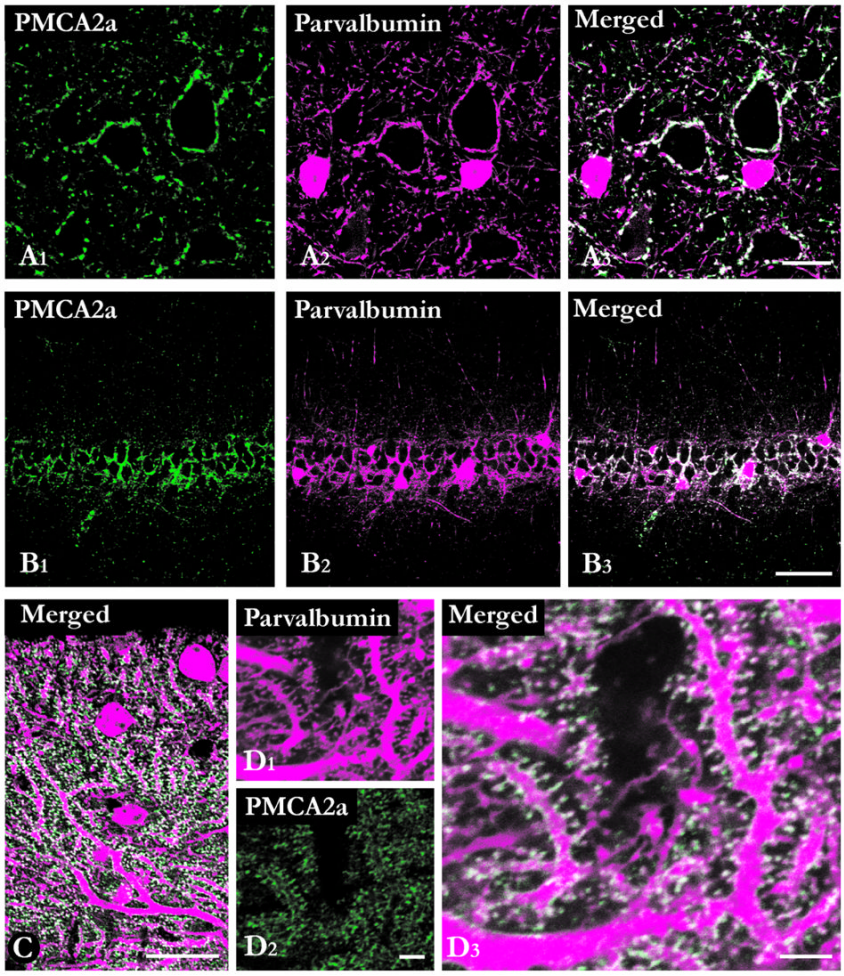

Figure 7.

Colocalization of PMCA2a with parvalbumin. Double labeling reveals extensive colocalization of PMCA2a with parvalbumin in cerebral cortex (**A**), hippocampus (**B**) and cerebellar cortex (**C,D**). In cerebral cortex and hippocampus colocalization is most prominent around cell bodies, presumably in axon terminals. In contrast in the cerebellar cortex, colocalization concentrates in dendritic spines. Scale bars = 10 μm in A,D; 50 μm in B; 25 μm in C.

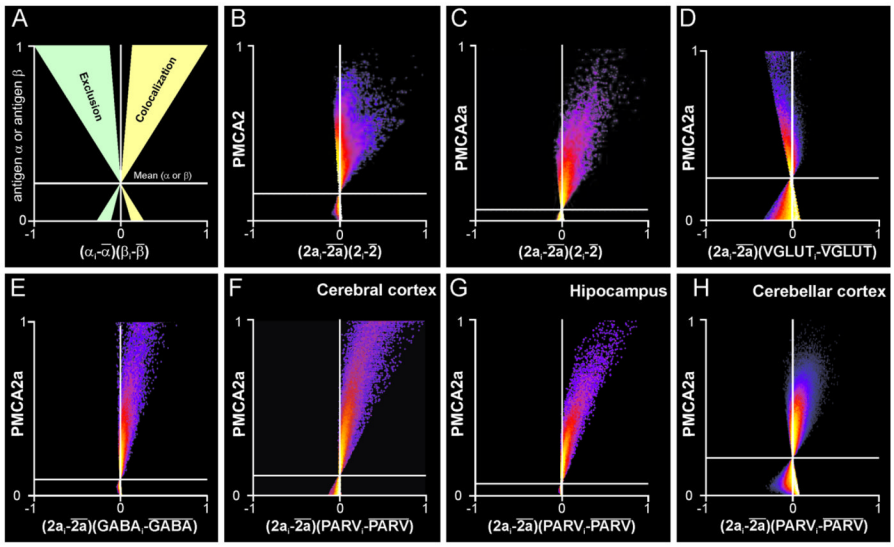

Figure 8.

Intensity correlation analysis of PMCA2a colocalization with different synaptic terminal markers. Analyses are presented as graphs where the x-value [(protein a intensity)–(mean protein a intensity)] [(protein b intensity)–(mean protein b intensity)] is dependent on covariance of both channels, and the y-value reflects the intensity distribution of the one of the two proteins. The color of each point in the graph represents the frequency of pixels that display those particular values in the graph, from blue (low frequency) to yellow (high frequency). Pixels with values situated left of the x = 0 line do not colocalize or have inversely correlated intensities, whereas pixels situated on the right side colocalize (**A**, for details, see Materials and Methods). The graph showing PMCA2 with respect to PMCA2a shows two clouds of points, one close to 0 and another skewed to the right (**B**), indicating that one fraction of PMCA2 staining is independent of PMCA2a (absence of colocalization) while a second, smaller fraction is strongly correlated with PMCA2a. In contrast, the plot for PMCA2a with respect to PMCA2 (**C**) is skewed toward positive values, indicating that most PMCA2a colocalized with PMCA2. The plot for PMCA2 and VGLUT (**D**) is skewed toward negative values, indicating an absence of colocalization. On the other hand, plots for PMCA2a with respect to GABA (**E**) and parvalbumin (**F–H**) are skewed toward positive values, indicating colocalization. Each scatterplot corresponds to optical sections used for illustrations in Figures 5, 6, and 7: B and C, Figure 5E; D, Figure 6A; E, Figure 6B, F, Figure 7A; G, Figure 7B; D, Figure 7C. The scatterplots are from raw confocal images, while contrast and brightness were adjusted in the final figures.